Accepted Article

Three-dimensionally hierarchical Pt/C nanocompsite with ultra-high dispersion of Pt nanoparticles as a highly efficient catalyst for chemoselective cinnamaldehyde hydrogenation

Duo Hu,[a] Wenqian Fan,[a] Zhi Liu*[a] and Ling Li*[a]

Abstract: A monolithic carbon-supported Pt nanocomposite with interconnected three-dimensionally hierarchical porous carbon framework and ultra-high dispersion of Pt nanoparticles (Pt/3DHPC) is synthesized using an effective "liquid phase impregnation template" strategy. The obtained Pt/3DHPC possesses rich mesoporosity and low amount of oxygen-containing functional groups, which notably improve accessible internal surface area of macropores, number of active Pt sites, and electron transfer ability. When used as catalyst for the selective cinnamaldehyde (CMA) hydrogenation towards cinnamyl alcohol (CMO), the Pt/3DHPC exhibits high CMA conversion (92.7%) and CMO selectivity (91.1%) at 1 h reaction time, and the corresponding activity (1553.7 h^{-1})
greatly surpasses not only the single-sized mesoporous carbon and microporous activated carbon supported counterparts but also the previously-reported Pt catalysts dispersed on other forms of carbon. Furthermore, the Pt/3DHPC can be reused at least fifteen times without pronounced decays due to the strong interaction between Pt and carbon. The present work demonstrates the validity of multiscale control in carbon-supported Pt catalysts *via* overall consideration of the mass transportation, and the accessibility, quantity and capability of active sites towards chemoselective hydrogenation of CMA, which is expected to be extended to other catalysis-related processes.

Introduction

As a fundamentally important additive or intermediate in food industry, perfumery, and pharmaceutical synthesis, cinnamyl alcohol (CMO) is commonly derived from the selective hydrogenation of C=O bond in cinnamaldehyde (CMA).[1] Unfortunately, the competitive C=C bond hydrogenation in CMA often occurs simultaneously to form the undesirable by-product of hydrocinnamaldeyde (HCMA) due to the higher binding energy of C=O bond than that of C=C bond and more favorable thermodynamical reduction of C=C bond than that of C=O bond (Scheme.1). Therefore, considerable efforts have been focusing on promoting the selectivity towards the desired product of CMO. Precious metal platinum (Pt) is the most extensively investigated and seems to be the most effective active specie for the selective hydrogenation of CMA towards CMO owing to its large *d*-band which leads to the strongly repulsive four-electron interaction with the C=C bond and strongly attractive interaction with the C=O bond.[2] On the other hand, support is also a nonnegligible factor to affect the yield of CMO. Carbon materials have been testified to be one of the best choices as the catalyst support for heterogeneous reactions in liquid phase due to its excellent mechanical strength and stability under hydrothermal conditions, good electronic properties, large surface area for dispersing active components, easy recovery-refining-recycling for precious metals, relatively low cost as well as versatile

existing forms.[3] Over the past years, various carbon-supported Pt (Pt/C) catalysts, including Pt/carbon nanotubes (CNTs),[4-10] Pt/graphite,[11] Pt/graphene,[12-14] Pt/carbon nanofiber,[7, 15-17] Pt/carbon aerogel and xerogel,[18, 19] Pt/mesoporous carbon,[20] Pt/ hollow carbon spheres,[21] have been investigated for hydrogenation of CMA towards CMO. Although enhanced performances in catalytic activity and selectivity can be achieved with these Pt/C catalysts, they often suffer from some intrinsic defects: (i) the relatively weak interactions between carbon scaffold with Pt as well as the sequent Pt detachment during the reaction, (ii) low Pt dispersion, (iii) random pore size distribution of catalyst for low efficiency of mass transportation, all of which enormously inhibit the fully active release of Pt. It is commonly recognized that chemoselective hydrogenation of CMA is a complex process involving gas-liquid-solid three-phase interface behaviour. Therefore, it is very essential to explore new fabrication methods for the new Pt/C catalyst to solve these drawbacks.
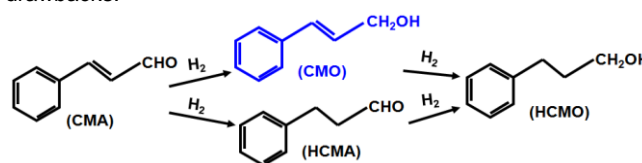
Scheme 1. Possible reaction pathway in hydrogenation of CMA.

In recent years, three-dimensionally hierarchical porous carbons (3DHPCs) with combined micropore or/and mesopore throughout a 3D-interconnected macroporous carbon skeleton have drawn increasing interests owing to their potential applications in catalysis, adsorption, CO_2 capture, energy storage/conversion, and drug delivery.[22-30] In contrast with the single-sized pore counterparts (microporous, mesoporous, or macroporous carbon), the 3DHPCs are expected to combine the advantages of each pore size regime. Particularly as catalyst supports, the monolithic macroporous skeleton is mechanically and thermally stable for facilitating the mass transportation of the

[a]   D. Hu, W. Q. Fan, Prof. Z. Liu, L. Li
         Faculty of Chemistry and Chemical Engineering
         Liaoning Normal University
         Dalian, Huanghe Road 850#
         E-mail: zhiliu@lnnu.edu.cn
                  lingl@lnnu.edu.cn

         Supporting information for this article is given via a link at the end of the document.

reactant and the product molecules. The mesopores in the macroporous walls can supply larger surface areas for the nucleation and growth of more active component, leading to higher activities and better-controlled selectivities, *i.e.*, the confinement effect of mesopore.[31] Conventionally, there are two typical approaches for fabricating the 3DHPCs. One is a two-step carbonization-activation method with coalderivatives,[32, 33] organic polymer,[34, 35] or biomass[36, 37] as carbon sources, and the other is the liquid phase impregnation template (LPIT) strategy, which involves filling the void space of a porous template with a variety of carbon-containing precursors followed by solidification of the precursors, removal of template, and pyrolysis under an inert atmosphere.[38-42] For the latter, it can be envisaged that the desired metal active species may be directly introduced into the 3DHPC solid-state nanoarchitecture through using the mixed solution containing corresponding metal salt and organic sol-gel as precursor to infiltrate the template, and thereby leads to a high metal dispersion and a uniform metal/carbon (host/guest) constitution. Moreover, the spatial hindrance caused by the carbon matrices can strictly prevent the aggregation, growth, and detachment of the metal active species during reaction. Although some of the active species might be entrapped or encapsulated by the carbon matrices resulting in the inaccessible to the reactant molecules and thus decreasing the intrinsic high catalytic activity of catalyst, the hierarchical micropores or/and mesopores in the walls of the macroporous framework would potentially ensure the catalytically active sites to be approached easily as much as possible and afford stability under repetitive recycling.[43]

On the basis of the above elaboration, we for the first time report the synthesis of a novel 3DHPC-supported Pt (Pt/3DHPC) nanocomposite by means of a multi-component (resorcinol-formaldehyde resol, triblock copolymer F127, and hydrochloroplatinic acid) infiltration of polymethyl methacrylate (PMMA) templates followed by a direct pyrolysis process. The as-prepared Pt/3DHPC possesses pore-hierarchical structure with an ultra-high Pt dispersion. Pt nanoparticles with an average size of 1.57 nm can be directly introduced into the carbon matrices, and F127 acts as a structure-directing agent to create mesopores in the 3DHPC skeletons and increase surface area for active sites. When the Pt/3DHPC is used as the catalyst in the selective liquid-phase hydrogenation of CMA, it exhibits higher CMA conversion and CMO selectivity than those of the single-sized mesoporous and microporous carbon-supported Pt counterparts (Pt/MC and Pt/MAC).

Results and Discussion

Figure 1a depicts the SEM image of the PMMA templates. It is observed that the PMMA templates have a uniform spheres arrays with an average diameter around 270 nm in a face-centered cubic close packed in a large-scale. No significant disordered region is observed over the entire surface. The Pt/3DHPC catalyst is obtained by filling the void of the colloidal PMMA templates with RF resol solution containing $H_2PtCl_6 \cdot 6H_2O$. Figure 1b depicts the typical SEM image of the resulting

Pt/3DHPC at a low-magnification. It is clearly seen that the Pt/3DHPC displays a relative intact and solid three-dimensional arrangement in an interconnected macroporous framework with distinct skeleton breakages and point defects. At a high-magnification (white rectangle zone in Figure 1b), the next layer of channel is highly visible through the macropores (Figure 1c). The voids are interconnected through open window, reflecting that the surface of the catalyst has a very enriching porosity. The macroporous size is ~180 nm, suggesting the occurrence of striking shrinkage of the PMMA templates during pyrolysis, which is possibly caused by the melting and carbonization of the PMMA microspheres and the sintering of the produced samples. [44]
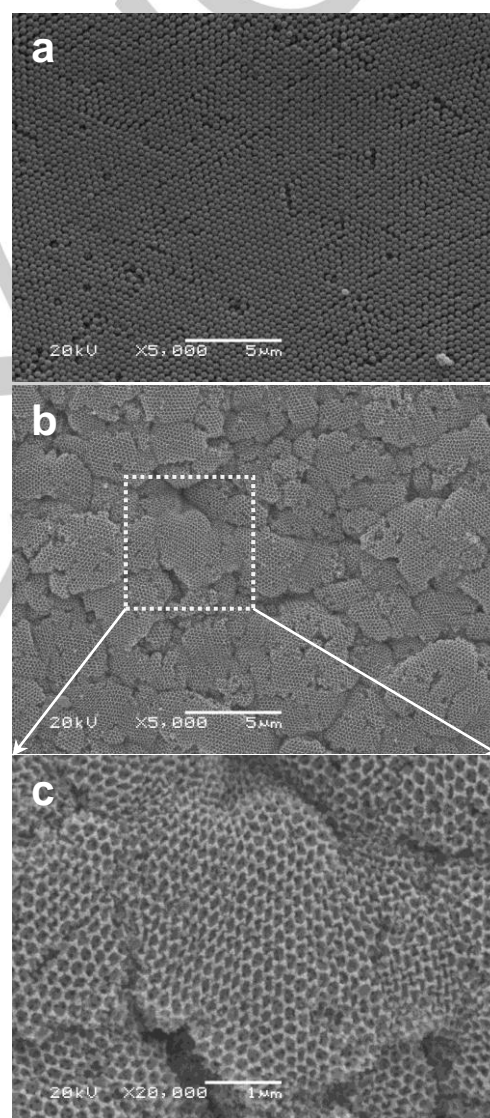

Figure 1. Typical SEM images of the PMMA template (a), Pt/3DHPC catalyst at a low-magnification (b), and Pt/3DHPC catalyst at a high-magnification (c).

Figure 2a reveals the N_2 adsorption-desorption isotherms and the corresponding PSDs of the Pt/3DHPC, Pt/MC, and Pt/MAC catalysts. It is found that the isotherm of Pt/3DHPC exhibits a combined characteristic of type I with type II. At the very low P/P_0, the adsorption amount increases sharply, indicating the presence of some micropores. The existence of a distinct H2 type hysteresis loop at medium P/P_0 (0.2-0.8) and no clear adsorption plateau at $P/P_0 \approx 1.0$ imply the presence of huge amounts of mesopores and macropores, respectively.[45-48] As shown in Figure 2b, the Pt/3DHPC possesses well-developed pore system with detectable sizes from 0.4 and 400 nm. The micropores with sizes of 0.4-2 nm and multiple peaks at 0.62, 0.86, 1.25, 1.46, 1.76 nm are possibly generated from the
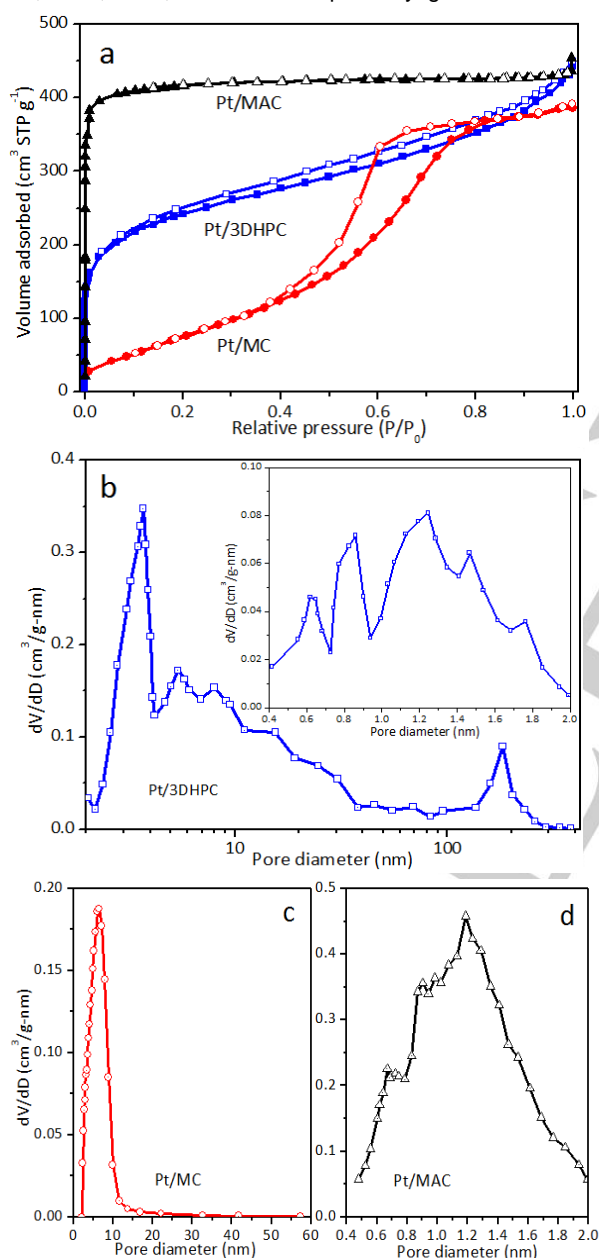
carbonization of the RF resol, whereas the mesopores with a broad distribution of 2-50 nm and a maximum peak at 3.7 nm is contributed from the aggregation of cross-linked carbon particles and the templating function of F127. In the macroporous range of >50 nm, the macropores predominantly center at 183 nm, collaborating well with the SEM observation. The Pt/MC shows a typical type IV isotherm with sharp capillary condensation steps at a $P/P_0 = 0.4$-0.8, characteristic of mesoporous materials.[49] The relative PSD is narrowly centered at around 6.2 nm (Figure 2c). The Pt/MAC presents a typical type I isotherm and a broad microporous distribution of 0.4-2 nm, reflecting its essentially microporous structure (Figure 2d). Table 1 summarizes the detailed textual properties of the three catalysts. The Pt/3DHPC exhibits a S_{BET} of 668 m^2 g^{-1} and a V_p of 0.57 cm^3 g^{-1}. Its V_{meso} and V_{mic} are 0.46 and 0.06 cm^3 g^{-1}, respectively, which are stemmed from the present of mesopores and micropores in the macropore walls of the HPC, further indicating its hierarchically porous structure. In contrast with the Pt/3DHPC, the Pt/MC has a lower S_{BET} of ~573 m^2 g^{-1} and a smaller V_p of 0.38 cm^3 g^{-1} with a V_{meso} of 0.37 cm^3 g^{-1} and a tiny V_{mic} of 0.01 cm^3 g^{-1}, further verifying its single mesoporosity. The Pt/MAC possesses typical textural properties of microporous materials with a high S_{BET} of 1337 m^2 g^{-1} and a large V_p of 1.24 cm^3 g^{-1}. The corresponding V_{meso} is almost negligible. In addition, ICP results demonstrate that the exact Pt contents in the three catalysts is 2.8 wt.%, 3.1 wt.%, and 3.0 wt.%, respectively.

Table 1. Textural properties of the Pt/3DHPC, Pt/MC, and Pt/MAC catalysts.

Catalyst	S_{BET} (m^2 g^{-1})	V_{meso} (cm^3 g^{-1})	V_{mic} (cm^3 g^{-1})	V_p (cm^3 g^{-1})	Pt conte (wt.%)
Pt/3DHPC	668	0.46	0.06	0.57	2.8
Pt/MC	573	0.37	0.01	0.38	3.1
Pt/MAC	1337	-	1.23	1.24	3.0

Figure 3 records the XRD patterns of the Pt/3DHPC, Pt/MC, and Pt/MAC catalysts. For the three samples, there are two typical broad diffraction peaks at 2θ = ~22° and ~43° indexed as amorphous carbon structure.[50, 51] Both Pt/MC and Pt/MAC exhibit distinct diffraction peaks at 2θ = 39.8°, 46.3°, and 67.5°, which are assigned to the (111), (200), and (220) planes of Pt(0) face-centered cubic structure (JCPDS 04-0802), respectively. There is no evidence of peak related to the oxide of Pt, implying that the Pt precursor (H_2PtCl_6) is completely reduced by H_2 treatment. The average particle sizes of Pt estimated by the Scherrer equation are 5.68 and 3.47 nm for Pt/MC and Pt/AC, respectively. Intriguingly for the Pt/3DHPC, no characteristic diffraction peaks belonging to Pt species are detected. Such a phenomenon is possibly due to the low content of Pt (2.8 wt.%) or the high dispersion of Pt nanoparticles with small sizes in the 3DHPC framework.
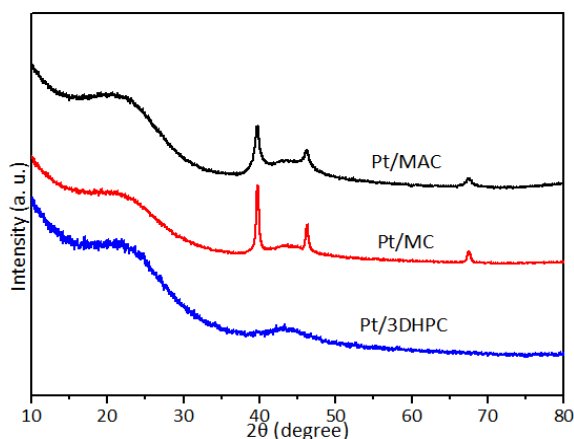
Figure 2. N_2-sorption isotherms (a) and corresponding pore size distributions of the Pt/3DHPC, Pt/MC, and Pt/MAC catalysts (b-d).

Figure 3. XRD patterns of the Pt/3DHPC, Pt/MC, and Pt/MAC catalysts.

Since the uncertainty of Pt valence, XPS is conducted to further identify the chemical state of Pt atoms as well as the elemental composition and heterocarbon components in the Pt/3DHPC, Pt/MC, and Pt/MAC catalysts, as shown in Table 2 and Figure S3. In the wide XPS survey spectra (Figure S3), there are three predominant peaks at around 74 eV (Pt 4f), 285 eV (C1s), and 531 eV (O1s), respectively, indicating the existence of not only the host carbon atoms but also Pt and O dopant atoms without evidence of impurities. On the high-resolution scan of the three catalysts (Figure 4a, 4c, and 4e), the asymmetric C 1s spectra can be deconvoluted into four individual component peaks, *i.e.*, the sp^2-hybridized C (C-C, 284.6 eV), the carboxyl, hydroxyl or ether C (C–O, 285.7 eV), the carbonyl or quinonyl C (C=O, 287.7 eV), and the carboxylate or lactone C (O=C–O, 289.0 eV), respectively.[52] The C–C functional group is the predominant carbon component (81.1%) in the Pt/3DHPC, other carbon species including the C-O (8.5%), C=O (5.1%), and O=C–O (5.3%) are presented with relatively low quantity (Table 2). Contrarily, the quantities of carbon atoms singly or doubly coordinated with oxygen atoms increase remarkably (7.8-19.3%) in both Pt/MC and Pt/MAC, accompanying with the decrease of the sp^2-hybridized C (53.7-60.8%) accordingly. These results indicate that most of oxygen-containing functional groups on the carbon surface of the Pt/3DHPC synthesized by the LPIT strategy have been thermally reduced during the RF resol pyrolysis with the stepwise-formed carbon itself as the reducing agent. While for the Pt/MAC and Pt/MC synthesized with the conventional support impregnation, there is still a certain amount of oxygen-containing functional groups on the carbon surface even after the following H_2 reduction (Table S2), which is highly disadvantageous to the dispersion of Pt. A more insightful understanding of this issue will be discussed in the following section for Pt XPS.

Figure 4b, 4d, and 4f show the XPS spectra of Pt 4f in the Pt/3DHPC, Pt/MC, and Pt/MAC catalysts. These spectra present two broad peaks, which can be fitted into two pairs of doublets with a spin-orbit splitting of $4f_{7/2}$ and $4f_{5/2}$ states, respectively. The major doublet with binding energies of 71.2 (Pt $4f_{7/2}$) and 74.5 (Pt $4f_{5/2}$) eV is attributed to metallic Pt (0),[53] whereas the minor one at 72.2 (Pt $4f_{7/2}$) and 75.6 (Pt $4f_{5/2}$) eV can be assigned
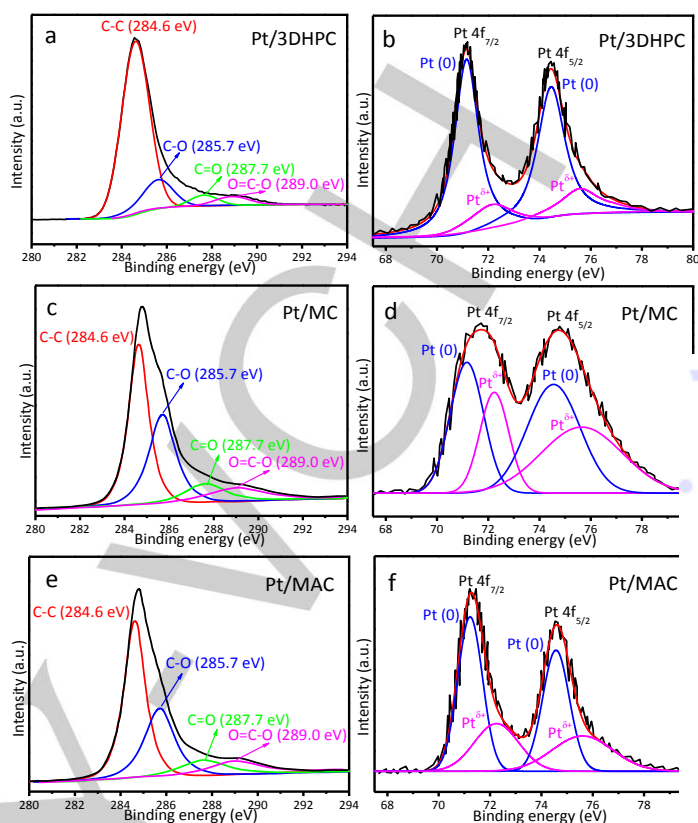

Figure 4. XPS spectra of C 1s (a, c, and e) and Pt 4f (b, d, and f) of the Pt/3DHPC, Pt/MC, and Pt/MAC catalysts.

to $Pt^{\delta+}$ chemical state that anchored with the oxygen-containing functional groups on the carbon surface (Pt-O-C).[54] The relative atomic percentages of the Pt (0) and $Pt^{\delta+}$ from the XPS spectra are also listed in Table 2. For the Pt/3DHPC (Figure 4b), Pt (0) exists in a high portion of 87.3%, and the left of 12.7% exists as Pt-O-C. Li *et al.* ever fabricated a Pt/graphene catalyst for hydrogenation of CMA through a deposit-chemical reduction method and achieved excellent catalytic performances with a CMA conversion of 92% and a CMO selectivity of 88% in isopropanol under 10 bar H_2, 60 °C, and 4 h.[14] They believed that the large fraction (61%, determined by XPS) of Pt (0) sites on the surface of the catalyst played an important role in obtaining the high CMO selectivity. In contrast, the present Pt/3DHPC possesses a higher potion of Pt (0) (87.3%), which should be conducive to the enhancement of CMO selectivity potentially. Quite different from the Pt/3DHPC, the portions of Pt-O-C in the Pt/MC and Pt/MAC increase remarkably (Figure 4d and 4f), accounting for 43.7% and 33.9%, respectively. The higher percentages of $Pt^{\delta+}$ on surfaces of Pt/MC and Pt/MAC are presumably originated from the higher concentration of oxygen species on their surfaces, as aforementioned in the C 1s spectra section. It tends to believed that a support with rich surface oxides may accelerate the increase of Pt particle size because the surface oxides can weaken the interaction between Pt and support, and thereby leading to a lower resistance to surface migration of Pt particles.[55] As a result, large sizes of Pt particle

would be formed on the support containing rich surface oxides. Based on these analyses, we therefore infer that the sizes of Pt on the 3DHPC might be much smaller than those on the MC and MAC. This would benefit the selective hydrogenation of CMA towards CMO.

Table 2. Distribution of functional groups derived from the XPS data in the Pt/3DHPC, Pt/MC, and Pt/MAC catalysts.

Sample	Relative atomic percentage (%)				Heterocarbon component (%)	Relative atomic percentage (%)	
	C-O	C=O	O-C=O	C-C		Pt (0)	Pt$^{\delta+}$
Pt/3DHPC	8.5	5.1	5.3	81.1	18.9	87.3	12.7
Pt/MC	18.1	19.3	8.9	53.7	46.3	56.3	43.7
Pt/MAC	16.9	14.5	7.8	60.8	39.2	66.1	33.9

Figure 5 illustrates the representative TEM images of the Pt/3DHPC, Pt/MC, and Pt/MAC catalysts. In the Pt/3DHPC (Figure 5a), the interconnected networks of three-dimensional structures with overlapped pores can be clearly observed. In its partial magnified image (Figure 5b), the macroporous diameter is observed to be around 180 nm, in good agreement with its SEM observation. Pt nanoparticles are ultra-highly dispersed in the macropore walls of the carbon framework without any aggregations into large clusters, as seen by the tiny, spherical, and black spots. Further high-resolution TEM investigation reveals that the distance between two adjacent lattice planes of the spots is measured approximately to be 0.227 nm (Figure 5d), coinciding well with the Pt (111) plane of crystalline Pt.[56] On counting 800 nanoparticles, the average size of the Pt nanoparticles is calculated to be ~1.57 nm, as shown in the corresponding size distribution histogram (Figure 5c). By contrast, Pt nanoparticles supported on MAC have a relatively poor dispersion, and the average particle size is enlarged to be ~3.25nm (Figure 5f and 5h). While for the Pt/MC, most of Pt nanoparticles are severely aggregated to large regiments onto the surface of MC as the yellow circular rings shown. The average particle size excluding the agglomerates is calculated to be ~5.53 nm (Figure 5e and 5g). This is presumedly attributed to the weak confinement effect of mesopore caused by the conventional support impregnation. With the additional observation of electron dispersion spectroscopy, the ultra-highly dispersed Pt element in the 3DHPC framework is further verified (Figure S4). Through the TEM observation, the Pt/3DHPC apparently possesses better Pt dispersion than the others, confirming the presumption of XRD observations (Figure 3) and in good coherence with the XPS analyses (Figure 4). The features of ultra-high dispersion and fine size of Pt nanoparticles of the Pt/3DHPC are critical for the enhancement in catalytic activity. Also, such phenomenon indicates that the LPIT strategy used in our case can effectively prevent the aggregation of Pt nanoparticles for the synthesis of Pt/3DHPC, *i.e.*, Pt nanoparticles are thermally stable. In the 3DHPC skeleton with uniform Pt-carbon constitution, carbon phase can limit the space for the growth of Pt nanoparticles and act as a nanoglue to prevent the Pt nanoparticles from aggregating and sintering, and thereby resulting in an ultra-high dispersion of Pt nanoparticles even after the pyrolysis.
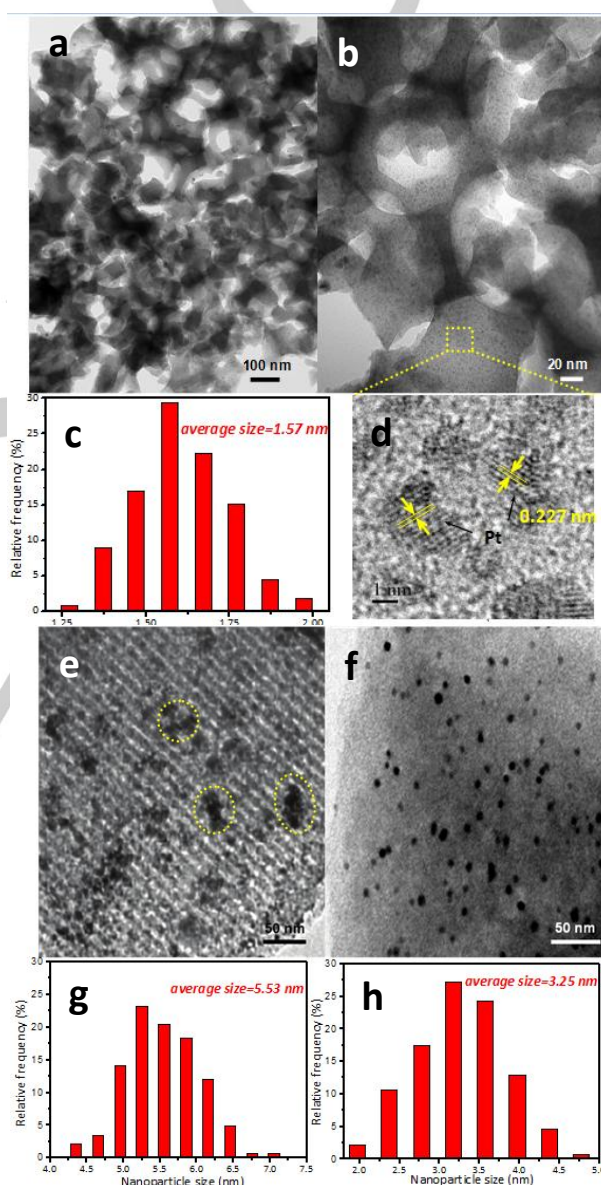

Figure 5. Representative TEM images the Pt/3DHPC catalyst at a low-magnification (a) and a high-magnification (b); particle size distribution of the Pt/3DHPC catalyst (c); high-resolution TEM image of the Pt/3DHPC catalyst (d); TEM image (e) and particle size distribution (g) of the Pt/MC catalyst; TEM image (f) and particle size distribution (h) of the Pt/MAC catalyst.

In order to further monitor the surface active sites and the intrinsic information regarding dispersion, H_2-chemisorption data are acquired on the Pt/3DHPC, Pt/MC, and Pt/MAC catalysts. As summarized in Table 3, the H_2 uptakes on the three samples is 41.9, 14.3, and 23.8 μmol/g_{cat}, respectively, following the order Pt/3DHPC > Pt/MAC > Pt/MC. The calculated Pt dispersions (D_{Pt}), 75.2%, 24.6% and 38.2%, also present the same sequence. Additionally, the dispersions are very close to those estimated with the average particle sizes by TEM (D_{TEM} = 1.133/d_{TEM}).[57] Because one H atom stoichiometrically chemisorbed on one Pt surface active site, the more H_2 uptakes, the more the number of the active sites has on the catalyst surface. This implies that the Pt nanoparticles loaded on the 3DHPC would be more enriching, and present more exposed and accessible active Pt sites than those on the MC and MAC. Evidently, the exceptionally good dispersion of Pt nanoparticles with 3D-interconnected hierarchical pore texture in the Pt/3DHPC can afford much more usable active sites and expectantly give rise to superior catalytic performance.

Table 3. H_2 chemisorption uptakes and the Pt dispersions of different catalysts.

Sample	H_2 chemisorption (μmol/g_{cat})	D_{Pt}[a] (%)	D_{TEM}[b] (%)
Pt/3DHPC	41.9	75.2	72.2
Pt/MC	14.3	24.6	20.5
Pt/MAC	23.8	38.2	34.9

[a] D_{Pt} was calculated by H_2 chemisorption data with a stoichiometry of H/Pt = 1/1. [b] D_{TEM} was estimated according to D_{TEM} = 1.133/d_{TEM}.

Selective hydrogenation of CMA towards CMO is a typical reaction for the conversion of α, β-unsaturated aldehydes into industrially important allylic alcohols. Precious metal (Au, Ir, Pt, and Pd) nanocatalysts have been widely investigated for this reaction and Pt has been proved to be more effective for the formation of CMO. On the other hand, some factors that influence the CMO selectivity, such as metal particle size, the support nature, and the adjunction of promoters, have also been taken into consideration significantly,[58] however, few reports deal with the effect of catalyst structures on the catalytic performances. In this work, with the success in the synthesis of Pt/C catalysts with different pore size regime, we can investigate the effect of catalyst structures on the reactivity in selective hydrogenation of CMA.

Table S3 lists the results for hydrogenation of CMA over the Pt/3DHPC, Pt/MC, and Pt/MAC catalysts. In the present work, three hydrogenation products of CMA, CMO, HCMA and HCMO are observed. Furthermore, acetals are also detected, meaning the occurrence of condensation of isopropanol and CMA. On the other hand, products from cracking or decarbonylation are not found. It is noted that the Pt/3DHPC exhibits a high CMA conversion of 92.7% at 1h reaction, which is far higher than those of the Pt/MC (45.1%) and Pt/MAC (43.7%) under the same reaction conditions. Meanwhile, the Pt/3DHPC possesses the highest CMO selectivity (91.1%), while the selectivities towards other products are quite low (3.9% for HCMA and 3.3% for HCMO). In contrast, CMO selectivity over the Pt/MAC is

much lower than that over the Pt/3DHPC (38.7%). On the contrary, its selectivity towards HCMO is the highest (40.6%) amongst the three catalysts, which is possibly attributed to the abundant microporous texture of the MAC (Table1) as discussed in Ref. 59. These micropores are huge obstacles for the effective diffusion of intermediate products of CMO from the catalyst, resulting in its successive hydrogenation to the saturated alcohol (HCMO). The Pt/MC with typical mesoporous structure makes the mass transportation relatively easier and shows a somewhat better CMO selectivity (53.4%). Based on these data, the calculated TOF value in terms of the amount of yielded CMO is 1553.7 h^{-1}, 1.3 and 2.7-fold of the Pt/MC (1224.0 h^{-1}) and Pt/MAC (571.8 h^{-1}), respectively. Clearly, the Pt/3DHPC catalyst remarkably outperforms the Pt/MC and Pt/AMC catalysts in selective hydrogenation of CMA towards CMO. Meanwhile, we also compare the CMA conversion, CMO selectivity, and TOF over the Pt/3DHPC with those over some previously reported carbon-supported Pt catalysts at the same reaction time of 1h. As tabulated in Table S3, our results for the Pt/3DHPC catalyst (92.7% CMA conversion with 91.1% CMO selectivity at 70 °C, 1h and 2.0 MPa H_2) apparently exceed most of the previously-reported counterparts with varied solvents and H_2 pressures. In addition, we conduct another reference test using a catalyst denoted as "Pt/3DHPC-im" (2.8 wt.% of Pt), which is prepared by the conventional support impregnation-hydrogen reduction with the as-prepared 3DHPC as support, as the Pt/MC and Pt/MAC. The corresponding sample characterizations are showed in Figure S5 and Tables S4. It is found that both CMA conversion (56.2%) and CMO selectivity (78.3%) over the Pt/3DHPC-im are much lower than those on the Pt/3DHPC (Table S3), which may be the result of the mesopore blockage with low efficiency of mass diffusion (Table S4) and relatively low Pt dispersion (42.4%) of the Pt/3DHPC-im further reflecting the advantages of the LPIT strategy.

The excellent catalytic performance of the Pt/3DHPC catalyst in hydrogenation of CMA can be understood as the following factors. As demonstrated in Figure 6, (i) in the macroscopical scale, the interconnected hierarchical porous carbon framework in the Pt/3DHPC can not only act as scaffolds to support and stabilize Pt nanoparticles but also provide more open channels, more accessible internal surface area, and thus more locations for Pt dispersion; the high porosity with hierarchical mesopores in the macroporous walls can facilitate the diffusion of reactant molecules of CMA and product molecules of CMO whose dimensional sizes are of *ca.* 0.90 nm × 0.51 nm × 0.08 nm and 0.98 nm × 0.51 nm × 0.29 nm, respectively, which is compatible with the pore range of the Pt/3DHPC (Figure 2b). To better understand the contribution of mass diffusion, the rate analyses are proceeded with different initial CMA concentration. By the fitting of linear equation, the reaction order is determined to be about 0.92, approaching to the theoretical reaction order of "1" for mass diffusion, and further confirming the great effect of hierarchical porous structure of the Pt/3DHPC on mass distribution and subsequent catalysis in our case (Figure S6). (ii) in the nano-scale, the ultra-high dispersion of Pt nanoparticles on the surface of 3DHPC can afford a high utilization efficiency of Pt with rich active sites. On the other hand, the Pt/3DHPC is
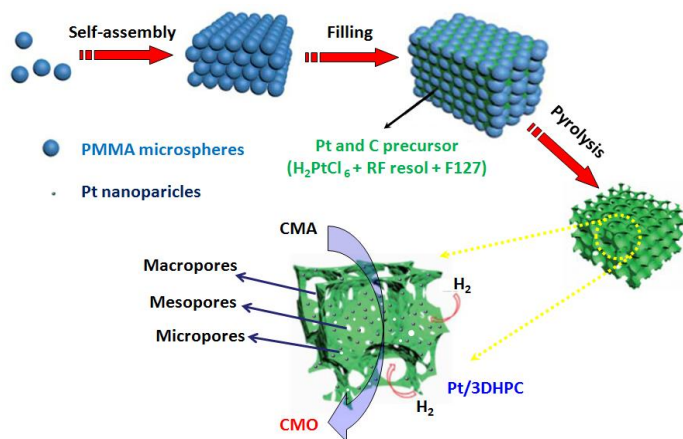
Figure 6. The proposed diagram for synthesis and selective CMA hydrogenation of the Pt/3DHPC catalyst.

synthesized by N$_2$-pyrolysis at 700 °C, which can eliminate most of the oxygen-containing functional groups on the formed 3DHPC surfaces (Tables 2), and subsequently produce outstanding electronic conductivity.[60] Vu *et al.* suggested that the conductivity of CNT was improved by removing electronegative oxygen atoms from the CNT surface, which enhanced the electron transfer from CNT to active Pt sites and reduced the probability of C=C bond coordinated to Pt active sites due to the electronic repulsion, thereby increased the CMO selectivity.[61] Yang *et al.* found that removal of oxygen-containing functional groups from CNT surfaces could elevate both CMA conversion and CMO selectivity, due to the suppressed side reactions catalyzed by acid and enhanced electron transfer from CNT to Pt nanoparticles.[8] According to these reports, we can infer that the Pt/3DHPC would have stronger ability in electron transfer between active Pt and carbon scaffold than the Pt/MC and Pt/MAC due to its less oxygen-containing functional groups (Tables 2 and S2). Furthermore, the Pt/3DHPC is monolithic with a relatively continuous network, which possesses smoother electronic conductivity than the irregularly cracked and loose-aggregated Pt/MC or Pt/MAC (Figure S7). Therefore, the electron is more easily transferred from the 3DHPC to the Pt centre, which favors the back-bonding interactions with $\pi_{C=O}$ to a larger extent than $\pi_{C=C}$, and thereby increasing the CMO selectivity.[2, 6] In addition, Su *et al.* reported that a series of Ru/C catalysts prepared by a thermal reduction method displayed a remarkably high catalytic activity and stability in benzene hydrogenation compared with Ru/C catalysts prepared by traditional impregnation-hydrogen reduction method.[62] They attributed such a high activity to the intimate interfacial contact between Ru particles and the carbon support. Szöllösi *et al.* applied ultrasonic irradiation to prepare a series of Pt-based catalysts for the hydrogenation of CMA to CMO, and found that the selectivity towards CMO with the smaller particle size of Pt was higher than the one with the larger particle size of Pt.[63] This difference in the selectivity was explained in terms of the formation of effective metal-support active centres, which provided strong acceptor sites for C=O adsorption. Gao *et al.* fabricated a series of hydrogenated MoOx (H-MoOx) and Mo$_2$C

supported Ir and Pt-Sn catalysts for some selective hydrogenation reactions, such as, CMA towards CMO,[64] crotonaldehyde towards crotyl alcohol,[65] and 4-nitrostyrolene towards 4-vinylaniline.[66] With the similar particle size and metal loading, they attributed the pronounced enhancements on both hydrogenation activity and selectivity of catalysts to the strong metal-support interaction, during which the reported novel supports (H-MoOx and Mo$_2$C) could donate (or gain) electrons to (or from) the active metal, and thereby giving rise to superior catalytic performance.In our case, the formation of Pt nanoparticles also originates from the thermal reduction with the carbon itself as the reducing agent, together with the formation of three-dimensionally hierarchical porous structure. Moreover, the Pt precursor (H$_2$PtCl$_6$·6H$_2$O) have been mixed uniformly with the carbon precursor (RF resol) before they are infiltrated into the interstices of the PMMA template arrays and then subjected to pyrolysis. Such one-pot formed Pt nanoparticles are mainly imbedded in or anchored on the 3DHPC walls, which would inevitably create intimate interfacial contact and strong interaction between the Pt nanoparticles and the carbon scaffold *i.e.*, substantial metal-support active centres and strong metal-support interaction. This can provide a similar microcosmic scenario in particle size and electron transfer as the reported catalysts. We can therefore infer that the smaller particle size of Pt (1.57 nm) with stronger ability of electron transfer in the Pt/3DHPC would contribute the higher CMO selectivity.In addition to the aforementioned factors, there might be other potential reasons for the high catalytic activity and selectivity of the Pt/3DHPC. Indeed, multistep reaction in heterogeneous catalysis is always a very complicated process, and the degree of the rate control of the elementary step might experience some changes over different catalyst formulations.[67, 68] This issue therefore deserves to be further explored.

The reusability is a fundamental parameter for precious metal catalysts from an economic point of view. Recently, Mao *et al.* synthesized a Pd@C catalyst *via* in *situ* entrapment of Pd nanoparticles in mesoporous carbon. The Pd nanoparticles with an average diameter of 3 ± 0.8 nm were largely encapsulated inside the mesoporous carbon channels without any serious aggregation. This catalyst exhibited excellent cycling stability without any significant loss of activity for 10 recycles in various heterogeneous hydrogenation reactions. They attributed the superior performance to the large surface area (S$_{BET}$ of 327.85 m^2 g^{-1}), high exposure of active Pd nanoparticles to the reactant, and the mesoporous pores allowing the reactants to easily access the catalyst without suffering large mass transportation resistance.[69] Compared with the reported Pd@C catalyst, the Pt/3DHPC in our case possesses not only an ultra-high dispersion of active Pt, but also more open three-dimensionally hierarchical structure with a uniform Pt-carbon constitution, a richer porosity (S$_{BET}$ of 668 m^2 g^{-1}), and a smoother mass transportation path, which would properly deserve a stronger reusability. Figure 7a indicates the cycle durability of the Pt/3DHPC catalyst under identical reaction conditions. To our delight, the catalyst can be easily recovered and shows no distinct decays in both CMA conversion and CMO selectivity even after fifteen cycles. These values begin to present a

decreased trend when the catalyst is subjected to the sixteenth use. This is likely stemmed either from the post-treatment (separation, ethanol wash, and drying out) for the used catalyst from the reaction system, which causes the gradual powdering of catalyst, or from the active Pt leaching during the recyclings. The ICP analysis of the catalyst after the fifteenth cycles reveals that only a trace amount of Pt leaching (<0.03 ppm) in solution is found, further reinforcing the strong interaction between the Pt nanoparticles and the carbon scaffold. The TEM image, XRD pattern, and XPS analysis (Figure S8-S10) also verify that the dispersion and crystalline state of Pt nanoparticles in the recovered Pt/3DHPC do not change significantly after fifteen cycles. In addition, the three-dimensionally hierarchical structure of the Pt/3DHPC is still maintained with partial pore distortion and damage to some extent, and the whole structural integrity remains considerably, as shown in Figure 7b. All of these results suggest that the Pt/3DHPC is economically suitable for repeating utilization.
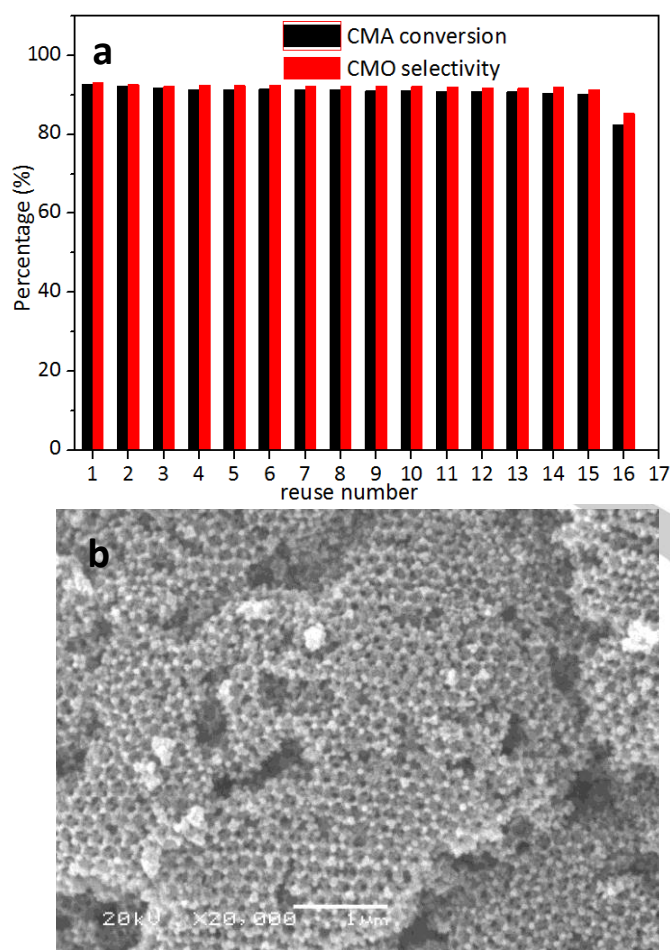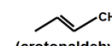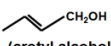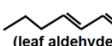
Because of the successful application of the Pt/3DHPC in hydrogenation of CMA reaction, it is therefore reasonable to conjecture that it would exhibit the versatility for hydrogenation of other α, β-unsaturated aldehydes to unsaturated alcohol. As listed in Table 4, these reactions proceeds extraordinarily well in a wide range of α, β-unsaturated aldehydes with various molecular configurations. For example, crotonaldehyde and leaf aldehyde appear to be very easy for hydrogenation with extremely high selectivities towards crotyl alcohol and *trans*-2-hexenol, respectively. As the molecular configuration of substrate becomes more complicated with longer carbon chain and larger substituents (citral and α-methylcinnamaldehyde), the increasing steric hindrance leads to relatively low conversion into the desired product.

Table 4. Hydrogenation of other α, β-unsaturated aldehydes to unsaturated alcohol over the Pt/3DHPC catalyst.

Entry	Substrate	Unsaturated alcohol	Conversion (%)	Selectivity
1	(crotonaldehyde)	(crotyl alcohol)	100	95.7
2	(leaf aldehyde)	(*trans*-2-hexenol)	100	94.4
3	(citral)	(geraniol) / (nerol)	96.5	91.2 (geraniol +
4	(α-methylcinnamaldehyde)	(α-methylcinnamyl alcohol)	85.6	87.7

Reaction conditions: 5 ml of α, β-unsaturated aldehydes, 70 °C, 2.0 MPa H₂, and 2h reaction
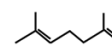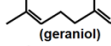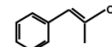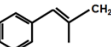

Figure 7. Reusability of the Pt/3DHPC catalyst for the hydrogenation of CMA towards CMO. Reaction conditions: 0.2 g of catalyst, 5 ml of CMA in 100 ml of isopropanol (reaction solvent), 2 MPa of H₂ pressure, 70 °C, and 2 h (a). SEM image of the Pt/3DHPC catalyst after completing 15 reuse (b).

Conclusions

In this work, we have successfully synthesized a monolithic Pt/3DHPC nanocomposite using an effective LPIT strategy with hydrochloroplatinic acid and resorcinol-formaldehyde resol as precursors and polymethyl methacrylate opal microspheres as template. Compared with the conventional support impregnation-hydrogen reduction, the direct integration of Pt and carbon in the three-dimensionally hierarchical porous nanoarchitecture enables such a nanocomposite to possess an ultra-high dispersion of Pt nanoparticles and strong interaction between the two components. For selective CMA hydrogenation towards CMO, the resulting Pt/3DHPC shows a high TOF up to 1553.7 h⁻¹, 1.3 and 2.7-fold activity of single-sized MC and MAC supported counterparts, respectively, and affords excellent reusability to fifteen time run. More importantly, our strategy opens up a meaningful platform for designing robust precious metal-based catalysts with an ultra-high dispersion for a broad range of applications in catalysis.

Experimental Section

Chemical agents: Pluronic F127 ($EO_{106}PO_{70}EO_{106}$) was supplied by Sigma-Aldrich and has an average molecular weight of 12,600. Methyl methacrylate (MMA), potassium persulfate ($K_2S_2O_8$), hydrochloroplatinic acid ($H_2PtCl_6 \cdot 6H_2O$, >37.5% Pt basis) and sodium hydroxide (NaOH) were purchased from Tianjin Kermel Chemical Reagent Co. Ltd. Resorcinol, formaldehyde (37 wt.%), hydrochloric acid (37 wt.%) (HCl), and ethanol were purchased from Shenyang Chemical Preparation Corp. All the chemicals were used as received without further purification. Deionized water was used in all experiments.

Synthesis of Pt/3DHPC: The polymethyl methacrylate (PMMA) colloidal crystal templates with an average diameter of ~270 nm were synthesized via a soap-free-emulsion polymerization based on Ref. 70. In a typical synthesis of Pt/3DHPC, 1.2 g of resorcinol (R) was dissolved in a solution containing 1.0 g of F127 and 7 g of ethanol/water (1:1 vol.%) under stirring until a brown solution was formed. Afterwards, 0.9 g of formaldehyde (F) was added dropwise to the above solution followed by an extra 3 h of stirring. Then, a desired amount of solution of $H_2PtCl_6 \cdot 6H_2O$ was added to the R/F127/F solution. The acid, formed from the ionization in the solution, was just utilized as the catalyst for RF polymerization. Next, the resulting solution composed of RF resol and $H_2PtCl_6 \cdot 6H_2O$ was added to a beaker containing the PMMA templates. Care was taken to keep the solution level below the top of the PMMA templates. Complete infiltration of the solution into PMMA templates occurred at about 12 h. After excess solution was wiped off the templates, these obtained pieces were heated in an oven at 100 ^{o}C overnight to induce thermal polymerization. Finally, the resultant was pyrolyzed under flowing N_2 at 400 ^{o}C for 3 h to remove the PMMA templates and then at 700 ^{o}C for another 2 h for RF resol carbonization with a heating rate of 1 ^{o}C min^{-1}. The as-synthesized sample was denoted as the Pt/3DHPC catalyst and the exact Pt content was determined by inductively coupled plasma (ICP) measurement.

Sample characterizations: The morphology and microstructure of samples were observed by a JSM 6360-LV scanning electron microscope (SEM) and a JEOL 2000EX transmission electron microscopy (TEM), respectively. Textural properties were measured by N_2-sorption at -196 ^{o}C on a Micromeritics ASAP 2010 apparatus. Before measurement, the samples were degassed firstly at 110 ^{o}C for 2 h and then at 300 ^{o}C for 3 h under vacuum. The specific surface areas (S_{BET}) of samples were calculated by the Brunauer-Emmett-Teller equation. The pore size distributions (PSD) and the mesopore volumes (V_{meso}) were derived from the desorption branches of the isotherms using the Barrett-Joyner-Halenda method. The total pore volumes (V_P) were estimated from the adsorption branches at a relative pressure (P/P_0) of 0.998. The micropore volumes (V_{mic}) were determined by the t-plot method. Powder X-ray diffraction (XRD) patterns were collected with a D/Max-βb diffractometer using Cu Kα radiation source (λ= 0.15432 nm). The exact Pt contents in samples were determined by an IRIS Intrepid II XSP instrument. X-ray photoelectron spectroscopy (XPS) was conducted on PHI Quantum 2000 equipped with an Al Kα radiation source. All binding energies (BE) were calibrated with graphitic carbon C1s peak at BE of 284.5 eV as a reference. H_2-Chemisorptions were performed using a Micromeritics AutoChem II 2920 instrument with a pulse chemisorption mode. For each measurement, a catalyst sample (100 mg) was firstly pre-treated by reduction in a pure H_2 flow at 400 ^{o}C for 1 h and purged with pure Ar for 1 h at the same temperature. After cooling to room temperature under Ar, the gas flow was switched to 10% H_2/Ar to start the H_2-chemisorption. H_2 loop gas was used for each pulse, and the adsorption was assumed to be completed until the thermal conductivity detector signals being constant.

Catalytic activity measurements: The CMA hydrogenation was carried out in a 150 mL custom-designed stainless autoclave with a Teflon inner layer. After the addition of 0.2 g catalyst, 5 ml CMA and 100 ml isopropanol (reaction solvent) were used. The selection of isopropanol was determined by advanced screening of reaction solvent (Table S1). Then the autoclave was sealed, and the air residue was expelled by pressurizing and releasing hydrogen several times. The reaction mixture was stirred with a magnetic stirrer at a rate of 900 rpm with a pre-optimization (Figure S1). The reaction was started when the required temperature was achieved, and was monitored by taking around 1.0 mL samples from the reaction mixture periodically to determine the conversion and selectivity. The reaction products were analyzed by a gas chromatography (Agilent 6890) equipped with a flame ionization detector and a 0.25 mm x 30 m FFAP capillary column (Figure S2). For comparison, commercial mesoporous carbon (MC) and microporous activated carbon (MAC) were used as supports for preparing Pt/MC and Pt/MAC catalysts by the conventional support impregnation-hydrogen reduction (see Supporting information for details). The exact Pt contents of the two catalysts were also determined by ICP.

Calculation of turnover frequencies (TOFs): The TOF, reflecting the conventional calculation of turnover frequency based on the metal dispersion, was calculated in order to compare the intrinsic activity of the Pt/3DHPC catalyst with others Pt-based catalysts in the previously reported literature in hydrogenation of CMA. The TOF is defined as the following equation:[18]

$$TOF = \frac{CMO_{yielded}}{t(m_{cat}X/M)D}$$

where $CMO_{yielded}$ is the mole of obtained CMO, t is the reaction time (h), m_{cat} is the amount of catalyst (g), X is the Pt content in the catalyst (wt.%) D is the Pt dispersion (%) calculated from H_2-chemisorption data or average particle size of Pt, and M is the molar weight of Pt (195.1 g mol^{-1}).

Acknowledgements

[1]   P. Gallezot, D. Richard, *Catal. Rev. Sci. Eng.* **1998**, *40*, 81-126.
[2]   F. Delbecq, P. Sautet, *J. Catal.* **1995**, *152*, 217-236.
[3]   M. M. Li, F. Xu, H. R. Li, Y. Wang, *Catal. Sci. Technol.* **2016**, *6*, 3670-3693.
[4]   H. X. Ma, L. C. Wang, L. Y. Chen, C. Dong, W. C. Yu, T. Huang, Y. T. Qian, *Catal. Commun.* **2007**, *8*, 452-456.
[5]   Z. T. Liu, C. X. Wang, Z. W. Liu, J. Lu, *Appl. Catal. A: Gen.* **2008**, *344*, 114-123.

[6] A. Solhy, B. F. Machado, J. Beausoleil, Y. Kihn, F. Gonçalves, M. F. R. Pereira, J. J. M. Órfão, J. L. Figueiredo, J. L. Faria, P. Serp, *Carbon* **2008**, *46*, 1194-1207.

[7] A. Jung, A. Jess, T. Schubert, W. Schütz, *Appl. Catal. A: Gen.* **2009**, *362*, 95-105.

[8] Z. Guo, Y. T. Chen, L. S. Li, X. M. Wang, G. L. Haller, Y. H. Yang, *J. Catal.* **2010**, *276*, 314-326.

[9] B F. Machado, H. T. Gomes, P. Serp, P. Kalck, J. L. Faria, *ChemCatChem* **2010**, *2*, 190-197.

[10] B. H. Zhao, J. G. Chen, X. Liu, Z. W. Liu, Z.. P. Hao, J. L. Xiao, Z. T. Liu, *Ind. Eng. Chem. Res.* **2012**, *51*, 11112-11121.

[11] E. V. Ramos-Fernández, J. M. Ramos-Fernández, M. Martínez-Escandell, A. Sepúlveda-Escribano, F. Rodríguez-Reinoso, *Catal. Lett.* **2009**, *133*, 267-272.

[12] J. J. Shi, R. F. Nie, P. Chen, Z. Y. Hou, *Catal. Commun.* **2013**, *41*, 101-105.

[13] Z. H. Sun, Z. M. Rong, Y. Wang, Y. Xia, W. Q. Du, Y. Wang, *RSC Adv.* **2014**, *4*, 1874-1878.

[14] X. W. Ji, X. Y. Niu, B. Li, Q. Han, F. L. Yuan, F. Zaera, Y. J. Zhu, H. G. Fu, *ChemCatChem* **2014**, *6*, 3246-3253.

[15] M. L. Toebes, Y. H. Zhang, J. Hájek, T. A. Nijhuis, J. H. Bitter, A. J. van Dillen, D. Y. Murzin, D. C. Koningsberger, K. P. de Jong, *J. Catal.* **2004**, *226*, 215-225.

[16] M. L. Toebes, T. A. Nijhuis, J. Hájek, J. H. Bitter, A. J. van Dillen, D. Y. Murzin, K. P. de Jong, *Chem. Eng. Sci.* **2005**, *60*, 5682-5695.

[17] A. J. Plomp, H. Vuori, A. O. I. Krause, K. P. de Jong, J. H. Bitter, *Appl. Catal. A: Gen.* **2008**, *351*, 9-15.

[18] B. F. Machado, S. Morales-Torres, A. F. Pérez-Cadenas, F. J. Maldonado-Hódar, F. Carrasco-Marín, A. M. T. Silva, J. L. Figueiredo, J. L. Faria, *Appl. Catal. A: Gen.* **2012**, *425-426*, 161-169.

[19] B. F. Machado, H. T. Gomes, P. Serp, P. Kalck, J. L. Figueiredo, J. L. Faria, *Catal. Today* **2010**, *149*, 358-364.

[20] P. V. Samant, M. F. R. Pereira, J. L. Figueiredo, *Catal. Today* **2005**, *102-103*, 183-188.

[21] I. Nongwea, V. Ravat, R. Meijboom, N. J. Coville, *Appl. Catal. A: Gen.* **2016**, *517*, 30-38.

[22] J. B. Zhang, L. J. Jin, Y. Li, H. H. Si, B. Qiu, H. Q. Hu, *Int. J. Hydrogen Energy* **2013**, *38*, 8732-8740.

[23] L. M. Zhang, T. T. You, T. Zhou, X. Zhou, F. Xu, *ACS Appl. Mater. Interfaces* **2016**, *8*, 13918-13925.

[24] G. Srinivas, V. Krunglevieiute, Z. X. Guo, T. Yildirim, *Energy Environ. Sci.* **2014**, *7*, 335-342.

[25] T. C. Chou, C. H. Huang, R. A. Doong, C. C. Hu, *J. Mater. Chem. A* **2013**, *1*, 2886-2895.

[26] S. C. Wei, D. T. Li, Z. Huang, Y. Q. Huang, F. Wang, *Bioresource Technol.* **2013**, *134*, 407-411.

[27] Y. P. Zhai, Y. Q. Dou, D. Y. Zhao, P. F. Fulvio, R. T. Mayes, S. Dai, *Adv. Mater.* **2011**, *23*, 4828-4850.

[28] H. Jiang, P. S. Leeb, C. Z. Li, *Energy Environ. Sci.* **2013**, *6*, 41-53.

[29] B. Z. Fang, J. H. Kim, M. S. Kim, J. S. Yu, *Acc. Chem. Res.* **2013**, *46*, 1397-1406.

[30] X. Y. Yang, L. H. Chen, Y. Li, J. C. Rooke, C. Sanchez, B. L.. Su, *Chem. Soc. Rev.* **2017**, *46*, 481-558.

[31] J. Su, J. S. Chen, *Micropor. Mesopor. Mater.* **2017**, *237*, 246-259.

[32] J. B. Zhang, L. J. Jin, J. Cheng, H. Q. Hu, *Fuel* **2013**, *109*, 2-8.

[33] J. B. Zhang, L. J. Jin, J. Cheng, H. Q. Hu, *Carbon* **2013**, *55*, 221-232.

[34] F. Xu, R. J. Cai, Q. C. Zeng, C. Zou, D. C. Wu, F. Li, X. E. Lu, Y. R. Liang, R. W. Fu, *J. Mater. Chem.* **2011**, *21*, 1970-1976.

[35] J. Yang, Y. Z. Bao, P. J. Pan, *Micropor. Mesopor. Mater.* **2014**, *196*, 199-207.

[36] S. Dutta, A. Bhaumik, K. C. W. Wu, *Energy Environ. Sci.* **2014**, *7*, 3574-3592.

[37] J. Deng, M. M. Li, Y. Wang, *Green Chem.* **2016**, *18*, 4824-4854.

[38] M. Yang, G. Wang, *Colloids Surf. A: Physicochem. Eng. Aspects* **2009**, *345*, 121-126.

[39] H. Xu, Q. M. Gao, H. L. Guo, H. L. Wang, *Micropor. Mesopor. Mater.* **2010**, *133*, 106-114.

[40] Y. D. Xia, Z. X. Yang, R, Mokaya, *Nanoscale* **2010**, *2*, 639-659.

[41] X. R. Wen, D. S. Zhang, L. Y. Shi, T. T. Yan, H. Wang, J. P. Zhang, *J. Mater. Chem.* **2012**, *22*, 23835-23844.

[42] M. J. Valero-Romero, E. M. Márquez-Franco, J. Bedia, J. Rodríguez-Mirasol, T. Cordero, *Micropor. Mesopor. Mater.* **2014**, *196*, 68-78.

[43] S. Ikeda, S. Ishino, T. Harada, N. Okamoto, T. Sakata, H. Mori, S. Kuwabata, T. Torimoto, M. Matsumura, *Angew. Chem. Int. Ed.* **2006**, *45*, 7063-7066.

[44] H. W. Yan, C. F. Blanford, B. T. Holland, W. H. Smyrl, A. Stein, *Chem. Mater.* **2000**, *12*, 1134-1141.

[45] J. J. Xu, Z. L. Wang, D. Xu, F. Z. Meng, X. B. Zhang, *Energy Environ. Sci.* **2014**, *7*, 2213-2219.

[46] J. Qin, Z. D. Cui, X. J. Yang, S. L. Zhu, Z. Y. Li, Y. Q. Liang, *Sensors Actuat. B: Chem.* **2015**, *209*, 706-713.

[47] Y. J. Zhang, J. G. Deng, H. Zhang, Y. X. Liu, H. X. Dai, *Catal. Today* **2015**, *245*, 28-36.

[48] H. G. Yang, J. G. Deng, Y. X. Liu, S. H. Xie, Z. X. Wu, H. X. Dai, *J. Mol. Catal. A: Chem.* **2016**, *414*, 9-18.

[49] J. M. Xu, A. Q. Wang, T. Zhang, *Carbon* **2012**, *50*, 1807-1816.

[50] Z. Liu, A. Q. Wang, X. D. Wang, T. Zhang, *Catal. Today* **2008**, *137*, 162-166.

[51] Z. Liu, Y. Yang, J. H. Mi, X. L. Tan, Y. Song, *Catal. Commun.* **2012**, *21*, 58-62.

[52] Q. Li, W. H. Xie, D. Q. Liu, Q. Wang, D. Y. He, *Electrochim. Acta* **2016**, *222*, 1445-1454.

[53] Y. M. Liang, H. M. Zhang, H. X. Zhong, X. B. Zhu, Z. Q. Tian, D. Y. Xu, B. L. Yi, *J. Catal.* **2006**, *238*, 468-476.

[54] J. Zhang, K. Sasaki, E. Sutter, R. R. Adzic, *Science* **2007**, *315*, 220-222

[55] M. Kang, Y. S. Bae, C. H. Lee, *Carbon* **2005**, *43*, 1512-1516.

[56] Q. Han, Y. F. Liu, D. Wang, F. L. Yuan, X. Y. Niu, Y. J. Zhu, *RSC Adv.* **2016**, *6*, 98356-98364.

[57] B. F. Machado, H. T. Gomes, P. Serp, P. Kalck, J. L. Figueiredo, J. L. Faria, *Catal. Today* **2010**, *149*, 358-364.

[58] S. Handjani, E. Marceau, J. Blanchard, J. M. Krafft, M. Che, P. Mäi-Arvela, N. Kumar, J. Wänåd, D. Y. Murzin, *J. Catal.* **2011**, *282*, 228-236

[59] P. H. Cuong, K. Nicolas, E. Gabrielle, L. J. Charbonniere, Z. Raymond, M. J. Ledoux, *J. Mol. Catal. A: Chem* **2001**, *170*, 155-163.

[60] J. Zhu, A. Holmen, D. Chen, *ChemCatChem* **2013**, *5*, 378-401.

[61] H. Vu, F. Gonçalves, R. Philippe, E. Lamouroux, M. Corrias, Y. Kihn, D. Plee, P. Kalck, P. Serp, *J. Catal.* **2006**, *240*, 18-22.

[62] F. B. Su, F. Lv, F. Y. Lee, T. Liu, A. I. Cooper, X. S. Zhao, *J. Am. Chem. Soc.* **2007**, *129*, 14213-14223.

[63] G. Szöllösi, B. Török, G. Szakonyi, I. Kun, M. Bartók, *Appl. Catal. A: Gen.* **1998**, *172*, 225-232.

[64] S. N. He, L. F. Xie, M. W. Che, H. C. Chan, L. C. Yang, Z. P. Shi, Y. Tang, Q. S. Gao, *J. Mol. Catal. A: Chem.* **2016**, *425*, 248-254.

[65] S. N. He, Z. J. Shao, Y. J. Shu, Z. P. Shi, X. M. Cao, Q. S. Gao, P. J. Hu, Y. Tang, *Chem. Eur. J.* **2016**, *22*, 5698-5704.

[66] Y. J. Shu, H. C. Chan, L. F. Xie, Z. P. Shi, Y. Tang, Q. S. Gao, *ChemCatChem* **2017**, DOI: 10.1002/cctc.201700880.

[67] C. Stegelmann, A. Andreasen, C. T. Campbell, *J. Am. Chem. Soc.* **2009**, *131*, 8077-8082.

[68] J. K. Nørskov, T. Bligaard, J. Kleis, *Science* **2009**, *324*, 1655-1656.

[69] H. Mao, S. J. Peng, H. Yu, J. Chen, S. L. Zhao, F. W. Huo, *J. Mater. Chem. A* **2014**, *2*, 5847-5851.

[70] L. J. Fu, T. Zhang, Q. Cao, H. P. Zhang, Y. P. Wu, *Electrochem. Commun.* **2007**, *9*, 2140-2144.

FULL PAPER
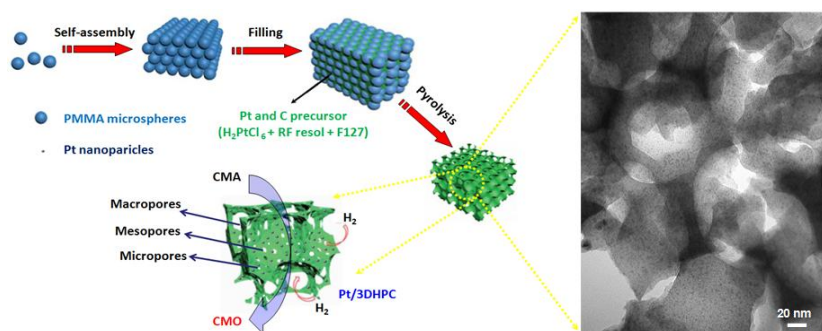
Duo Hu, Wenqian Fan, Zhi Liu*, and Ling Li*

Page No. – Page No.

Three-dimensionally hierarchical porous Pt/C nanocompsite with ultra-high dispersion of Pt nanoparticles as a highly efficient catalyst for chemoselective cinnamaldehyde hydrogenation

Ultra-high dispersion of Pt nanoparticles synthesis: A three-dimensionally hierarchical porous Pt/C nanocompsite with ultra-high dispersion of Pt nanoparticles is synthesized by means of an effective multi-component infiltration of polymethyl methacrylate templates. Pt nanoparticles are ultra-highly dispersed in the wall of the carbon scaffold and give rise to sufficient active sites for the cinnamaldehyde hydrogenation. The interconnected hierarchical porous carbon framework facilitates the diffusion of reactant molecules of cinnamaldehyde and product molecules of cinnamyl alcohol.